Eurasian Chemical Communications

SAMI

FULL PAPER

Numerical calculation of necessary distancing regarding SARS-CoV-2 (COVID-19) vs. spherical viruses, based on environmental features

Mohammad Javadi 🆔

Department of Mechanical Engineering, Quchan University of Technology, Quchan, Iran

Corona viruses are spherical nanoparticles with peripheral spike protein and diameters around 60 to 140 nm. In contrast to the elder versions, COVID-19 spread vastly and quickly all over the world. World Health Organization (WHO) insists on adequate social distancing in order to decrease the risk of contagion by air. In the present work, different parameters which affect the necessary social distance were investigated. Drag coefficient around a Corona-shaped nanoparticle with the geometry of COVID-19 was determined by modeling laminar flow in different Reynolds numbers. Accordingly, modified correlations for drag coefficient were derived which implied to be much higher in Corona-shaped particles in compare to spherical ones. Applying the new modified correlation, the behavior of 120 nm to 120 μm droplets generated by sneezing or coughing were investigated considering the evaporation of the volatile portion of the virus (around 94%), in different ambient conditions, namely temperature, pressure and relative humidity. Studying COVID-19 falling behavior showed that terminal velocity in Corona-shaped particles was much lower than spherical particles of the same size. It was also proved that falling time in Corona-shaped particles was longer, i.e. lasted longer in air. Ambient temperature increase and decrease in ambient relative humidity resulted into decrease in falling speed of the Corona particles. Decrease in ambient pressure, i.e. increase in elevation from sea level, yielded an increase in molecular free mean path which consequently resulted into reduction in falling speed. Hot dry areas were recognized to be critical from the viewpoint of COVID-19 spread through air.

*Corresponding Author:
Mohammad Javadi
Email: Mohammad.Javadi@qiet.ac.ir
Tel.: +989153155382

KEYWORDS

Introduction

Coronaviruses (COVs), categorized as Coronaviridae, are also characterized as pleomorphic RNA viruses containing crown-shaped peplomers with a size of 80-160 nm and a positive polarity of 32 kb [2-4]. These zoonotic pathogens are transferred to human and animal bodies at a very high mutation rate; they cause a wide range of clinical issues from asymptomatic course to severe intensive care unit (ICU) treatments due to respiratory infection and disruptions in the gastrointestinal, hepatic, and neurologic systems. COVs spread from person to person through the droplets produced by the infected person's sneeze or cough; consequently, they multiply and survive like any other living organism. They are transferred to the

respiratory system through mucous membranes, such as eyes, nose, or mouth.

The novel version of coronavirus, called COVID-19, was first recognized in Wuhan City, Hubei, China, and soon spread very rapidly throughout the world. In contrast to the older versions, such as SARS, MERS, and the flu, despite all similarities, COVID-19 spreads much more rapidly; this may be attributed to the various incubation periods [5]. Similar to the flu, the incubation period of COVID-19 is 1-14 days [1,6]. The long life cycle of the virus and its resistance against ambient conditions, particularly solar irradiation, plays an essential role in spreading.

Viruses are affected by temperature, pH, saltiness, and organic compounds. The flu can sometimes last longer than 100 to 200 days in distilled water based on the water temperature. Hepatitis virus can resist for 7 days at low temperatures and humidity and for 2 hours at high temperatures and humid areas [7]. Research on temperature and humidity effects shows that coronavirus lives longer (about 6 days) in 50% humidity compared to 30% and 80%. It has also been reported that after 24 hours, 80% of the viruses survive at 6 °C and only 3% at 20 °C [1,7].

Several pieces of research have been carried out on the life span of viruses and their contagion. Understanding the behavior of COVID-19 in air helps discover effective methods for disinfecting and preventing virus contagion. Several studies are dedicated to investigating the behavior and contagion of viruses generated from sneezing and coughing in different ambient conditions by computational fluid dynamics (CFD). These studies are categorized into 1) those investigating and tracking the virus path inside the body, spreading out from the mouth and nose [8-15] and 2) studies which focus on virus spreading in outdoor spaces such as classrooms, hospitals, airplanes, and public vehiclesand the role of mechanical ventilation systems on contagion restriction [16-23]. In 2005, Li et al. investigated the effect of air distribution on the spread of SARS virus in hospitals [23].

In 2011, Chaung et al. investigated the distribution and spread of air returning from isolated rooms in hospitals and its effect on virus contagion [20]. Lu et al. studied the effect of different parameters on the behavior of SARS virus detergents in 2015 [23]. Various CFD studies have been recently conducted on the spreading behavior of COVID-19 in urban environments [15,21,24,25]. In 2020, Blocken et al. studied the necessary social distancing during walking and running to avoid COVID-19 contagion [24]. They modeled the spray of water droplets, ranging from 70 to 600 μm, in an ambient temperature of 35 to 45°C and a relative humidity of 35% to 45%. In all the present numerical and experimental studies, the COVID-19 virus was modeled as a spherical water particle that was sprayed. Kotb et al. .simulated airflow and airborne particulates in the airplane cabin [18]. They modeled how passengers would affect air distribution inside the cabin. However, they made use of the existing default drag models in the Fluent for their simulations.

Studies performed before 2020 often concentrated on the spread of SARS while ignoring the special shape, dimensions, and size change of the virus produced by sneezing or coughing during settling. Coronaviruses are spherical particles with several peripheral spikes (Figure 1).
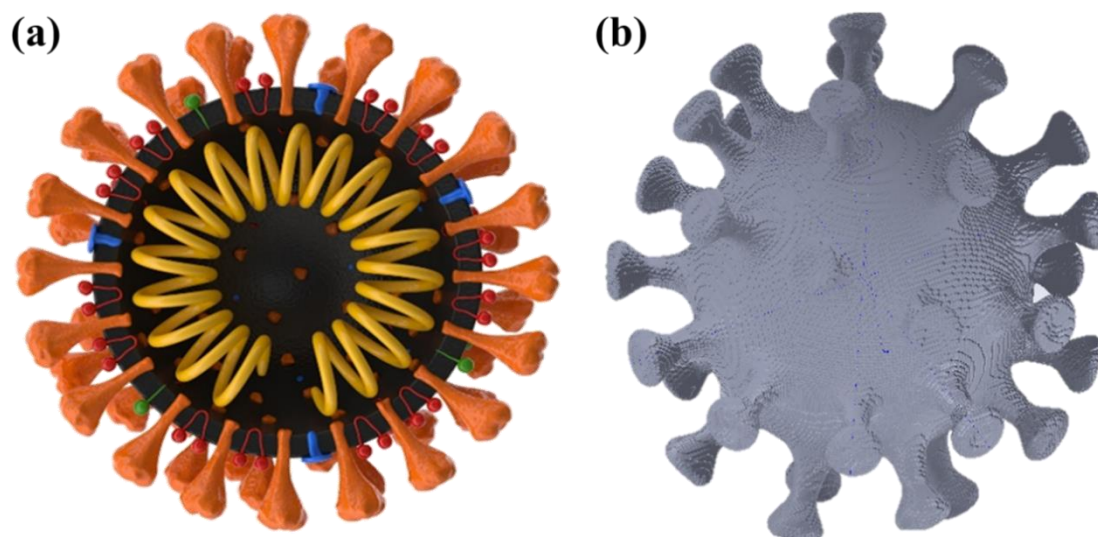
FIGURE 1 Coronavirus a) schematic [26], b) modeled geometry

This specific shape yields the ratio of surface area to volume around 10%, which is less than 6% in the spherical particles of the same size. The front area against the flow is also 25% larger than the equivalent spherical particle, positively influencing the terminal velocity and drag coefficient. Droplets spreading from sneezing or coughing include mucus with around 94% water content; these droplets are ten times bigger than the virus particles and can be assumed spherical. However, only the particles of a virus size and nonvolatile portions remain due to the high evaporation rate. Therefore, ignoring their actual size may result in significant modeling errors; this reduces the precision of investigation, especially at low-speed flows (low Reynolds numbers) such as that induced by temperature difference or natural convective flows with small temperature gradients. Determining the actual drag coefficient of corona-shaped particles can significantly help design efficient air change and ventilation systems in health centers to prevent viruses from spreading through the air. Hence, in this paper, the flow around the COVID-19 virus (with its actual geometry) was numerically modeled for various Reynolds numbers in order to derive the relevant drag coefficient correlations. Considering ambient pressure changes caused by altered elevation, hence the changes in the molecular free mean path, the correlations were modified via applying the slip correction factor in below-micron scale particles. Terminal velocities and fall time were investigated with respect to the modified drag coefficient correlations and evaporation rate in various humid conditions, ranging from 0% to 100%.

Numerical models

In the current work, numerical modeling was implemented in two steps as will be illustrated in the next sections. Primarily, the flow around the corona-shaped particles was numerically simulated, and the relevant drag coefficient was derived. Afterwards, by applying the new modified correlations, different ambient parameters influencing the droplet evaporation rate were modeled.
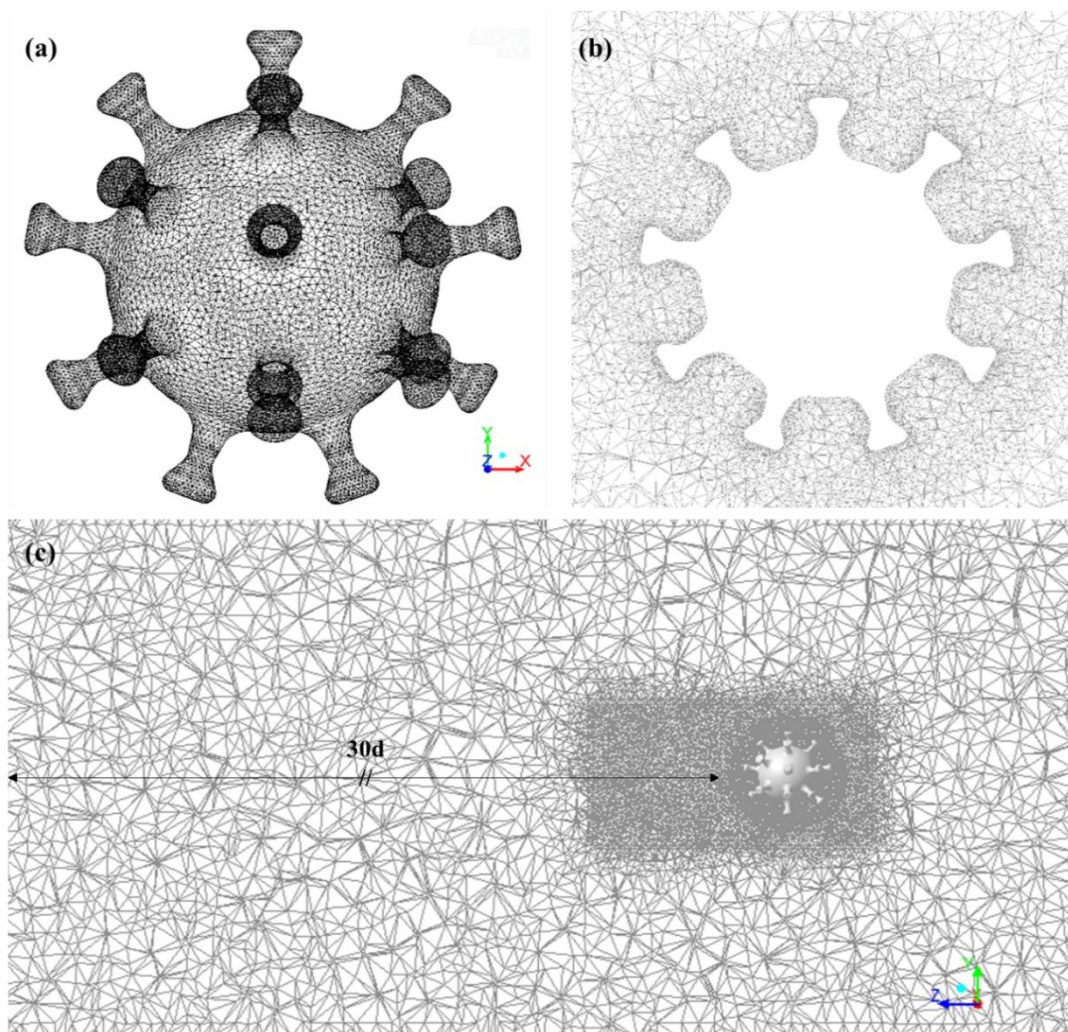
FIGURE 2 Computational grid of a) the virus surface, b) COVID-19 surroundings, c) the solution domain

A three-dimensional droplet of 120 nm diameter was employed for geometrical molding according to different references. Solution domain was extended 30d (30 times the droplet diameter) upstream and 20d from other directions (Figure 2b) in order to ensure the far-field flow was not bounded with the geometry presence. Mesh independency study indicated an unstructured computational grid of 1004749 tetrahedral cells with 34257 triangular nodes on the virus side area. As depicted in Figure 2, the computational grid was enlarged and extended several times around the droplet.

To study the independence of the results and the numerical simulation from the computational grid, boundary conditions corresponding to the spike protein changed from the wall to the interior, implying a sphere geometry (envelope). The results showed a good agreement with the governing analytical correlations on the flow around the sphere [27,28], proving the validity of the model. To calculate the drag coefficient, the Navier-Stokes equations for the incompressible steady state laminar flow [29] were numerically solved with double-precision using FLUENT Software.

b) The effect of ambient parameters on the droplet evaporation rate

In order to investigate the effect of ambient parameters, meaning temperature, pressure,

and relative humidity, the transport equation associated with three species of O_2, N_2, and H_2O, coupled with the above-mentioned flow equations, were numerically solved in a 3x3x5 m domain. To track the path of the droplets containing the virus (produced by breathing, sneezing, and coughing) in the air, the Lagrangian method and Discrete Phase Model (DPM) were applied. The drag coefficient around the particles was modified through a user-defined function (UDF).

Furthermore, the transient governing equation on the droplet evaporation [3,29-31] was solved, and the droplet diameter along the path was determined. The evaporation of the droplets is initiated once their temperature exceeds T_{vap} and stops either when their temperature reaches $T_{boiling}$ or the volatile part of the droplet completely evaporates. The volatile portion of the droplets produced by

sneezing or coughing is usually considered 94% [3]. Due to the small flow rate of the propagation of the droplets [3], their effects on the gaseous phase is ignored in simulations. Many researchers have employed the RNG k-ε model to apply the effect of turbulence on momentum equations for the same problems [3,32-34].

Results and discussion

In the current work, the flow around a particle with the same geometry as that of COVID-19 was numerically modeled. Drag coefficient in low Reynolds numbers was specified and compared with the spherical particles for the numerical simulation validation. An UDF then modified the drag coefficient in the DPM model.
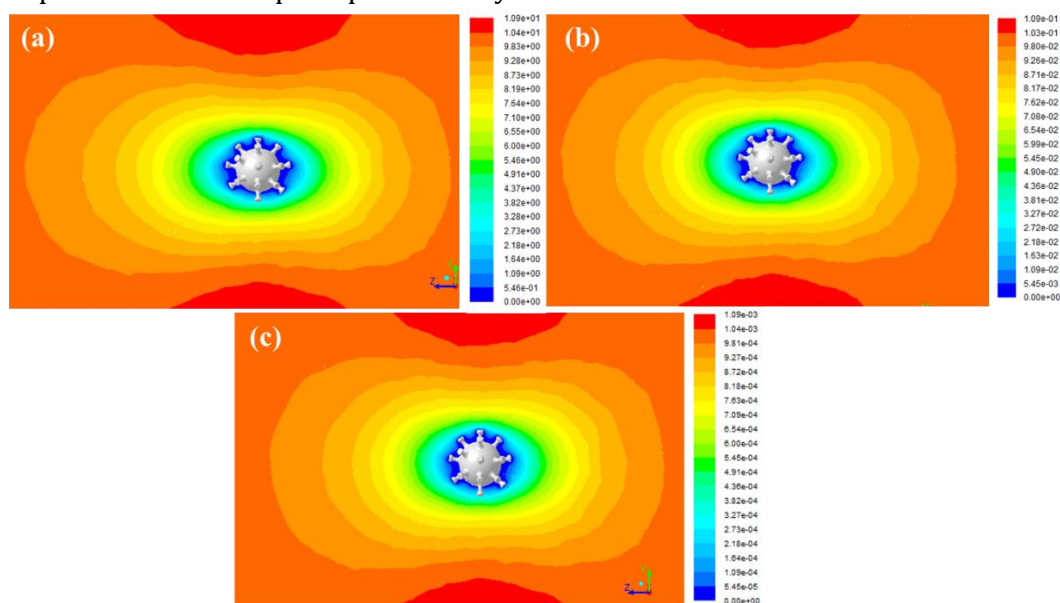

FIGURE 3 Velocity distribution around the particle a) $Re = 8.22 \times 10^{-2}$, b) $Re = 8.22 \times 10^{-4}$ and c) $Re = 8.22 \times 10^{-6}$

a) Flow filed and drag coefficient

Velocity distributions around the nanoparticle, COVID-19, are displayed in Figure 3 for $Re = 8.22 \times 10^{-2}$, 8.22×10^{-4} and 8.22×10^{-6}. As expected, symmetric streamLines were formed in the upstream and downstream of the particle without any

separation, which is similar to the flow around the sphere in $Re < 4$ [24].

Figure 3 Velocity distribution around the particle a) $Re = 8.22 \times 10^{-2}$, b) $Re = 8.22 \times 10^{-4}$, and c) $Re = 8.22 \times 10^{-6}$.

The drag coefficient of COVID-19 nanoparticle, determined by a three-dimensional laminar numerical simulation, is

plotted and compared with the sphere drag in Figure 4. For $Re < 0.1$, a similar trend (linear trend in logarithmic scale) can be observed in both COVID-19 and sphere. However, the COVID-19 particle yielded a higher drag coefficient compared with the spherical particles (approx. 1.5 time higher) due to their higher specific surface area* as predicted. Because of the virus diameter, their Reynolds number was too small to travel in the air ($Re_d \ll 1$). However, it is also concluded that the drag coefficient pattern for high Reynolds numbers ($Re_d > 1$) is approximately identical between the corona-shaped and spherical particles. Hence, assuming the geometry of the virus as a sphere will not result in noticeable errors in computations. Considering Figure 4, the following correlations can be presented for the drag coefficient of corona-shaped particles such as COVID-19 in different flow conditions. As seen, drag coefficient of Crona-shape particles are about 1.5 time higher than spherical particles in $Re < 1$, which accounts for simpler displacement of particles with vertical and horizontal flows. Simpler displacement with horizontal flows implies an increase in virus spread during fall. On the other hand, higher drag coefficient in vertical displacement results into an increase in drag force in compare to weight force, and consequently raise in fall time. Therefore, it is concluded that Crona-shape particles show more tendency to horizontal displacement under dominant flow conditions and also higher spreading rate due to molecular diffusion and turbulence, in compare to spherical particles. Hence, higher spreading rate and longer social distance than spherical particles are expected for Crona- shape particles.
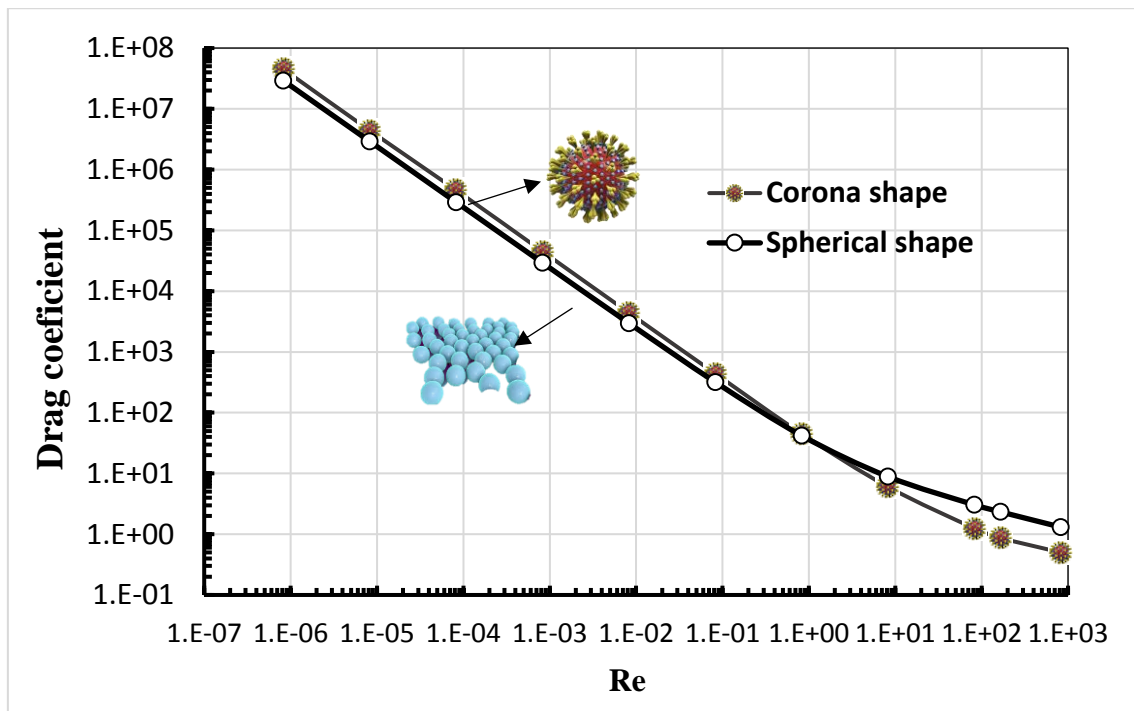

FIGURE 4 Comparison of the drag coefficient in corona-shaped and spherical particles of the same diameter for different Reynolds numbers

$$C_D = 36.3 Re^{-1.002} \quad ; \quad R^2 = 1 \qquad \text{for } Re \leq 1 \qquad (1)$$
$$C_D = 51 Re^{-0.964} \quad ; \quad R^2 = 0.9998 \qquad \text{for } 1 < Re \leq 100 \qquad (2)$$
$$C_D = 6.67 Re^{-0.338} \quad ; \quad R^2 = 0.9979 \qquad \text{for } 100 < Re < 1000 \qquad (3)$$

---

* Surface area for a specific particle diameter

The effect of slip in below-micron scale particles (particles smaller than the micron) is not considered in equations 1 to 3. Since the drag coefficient of these particles depends on the free mean path of air molecules, drag is modified by the Cunningham equation [27]. Given the high dependency of the free mean path on pressure, the modified drag coefficient of below-micron scale particles is plotted in Figure 5 for different ambient pressures, ranging from 78 kPa (7000 m above the sea level) to 114 kPa (>7000 m). Thus, for 120 nm particles, drag was approximately changed by 27% in the foregoing pressure range compared with the atmospheric pressure,

which can affect the terminal velocity. Figures 6 and S.1 show the terminal velocity variations with ambient temperature for 120 nm and 240 nm corona-shaped particles, respectively. As observed, terminal velocity increased with the rise in ambient temperature to 313K because of increased dynamic viscosity. The increase in the mean free path of the air molecules caused by pressure raise increased the slip factor, thereby reducing the drag coefficient. Comparison of Figures 6 and 7 showed a two-fold increase in the diameter of the corona particle, resulting in an approximate eight-fold increase in the terminal velocity.
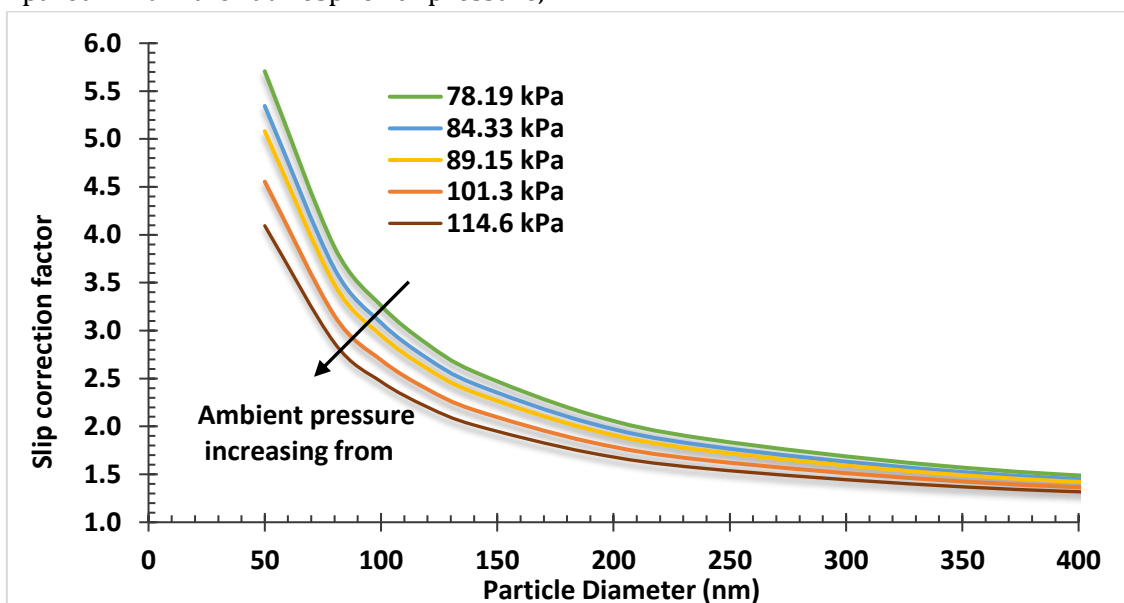

FIGURE 5 Variations in slip correction factor for below-micron scale particles in air for different ambient pressures.

Figure 6 compares the terminal velocity of the 120-nm diameter corona-shaped particles with that of the spherical particles at different ambient pressures and temperatures. Based on the results, the terminal velocity of the spherical particles was 1.4 times higher than that of the corona-shaped particles with the same diameter; this indicates the higher ratio of surface area to weight in corona-shaped

particles. Of note, considering coronavirus as having spherical particles can entail major errors, misleading the propagation modeling. For instance, Figure 9 illustrates the fall time from 1 m elevation for corona-shaped and spherical particles of the same diameter. It can be understood that corona-shaped particles drifted down 1.47 times slower than the spherical particles.
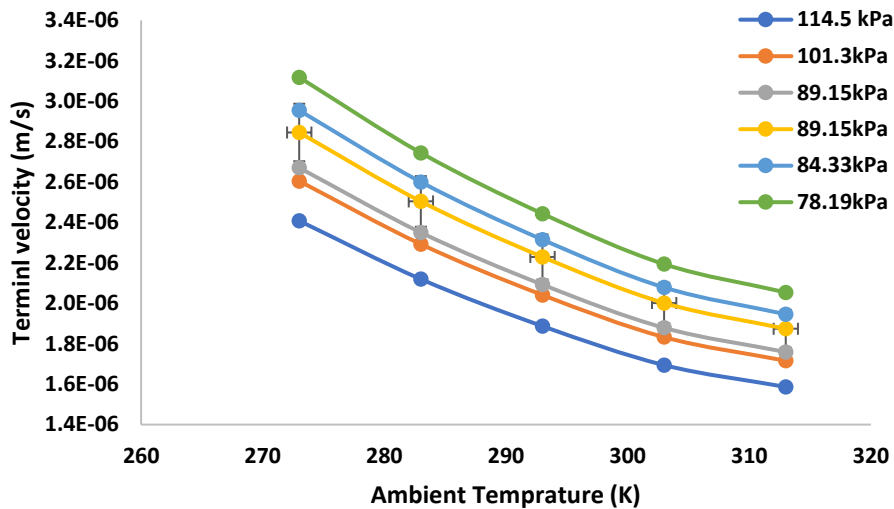
FIGURE 6 Effect of ambient pressure on the terminal velocity of a 120 nm corona-shaped particle at different ambient temperatures

Figure 8 compares the terminal velocity and fall time of corona-shaped and spherical particles from 120 nm to 200 nm. As seen, the decrease in particle diameter increased the fall time (per meter), thus playing a significant role in specifying the social distance. When exposed to horizontal wind, particles travel a distance before falling, called the fall time function. For instance, if particle velocity and flow velocity are assumed to have the same velocity of the below-micron scale and ignoring turbulence and vortexes in the flow and the death of the virus due to solar irradiation or other causes, a 120 nm particle can travel a distance as long as hundreds of kilometers with wind before falling. Displaced distances before falling were 40 km and 2 km for 1000 nm and 2000 nm particles, respectively.

Particles produced by sneezing or coughing are of micron-scale. However, their liquid portion (around 94% of respiratory mucosa weight) rapidly evaporates, causing the virus and their non-evaporative portion (if it exists) to continue the path and suspend for a long time.
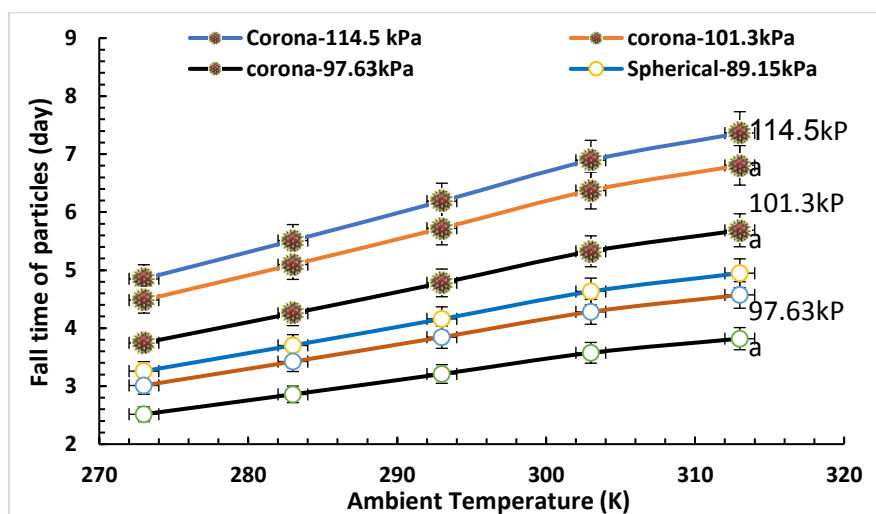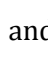

FIGURE 7 Fall time of 120 nm corona-shaped (🦠) and spherical particles (◯) in different ambient conditions from 78.2 kPa to 114.5 kPa
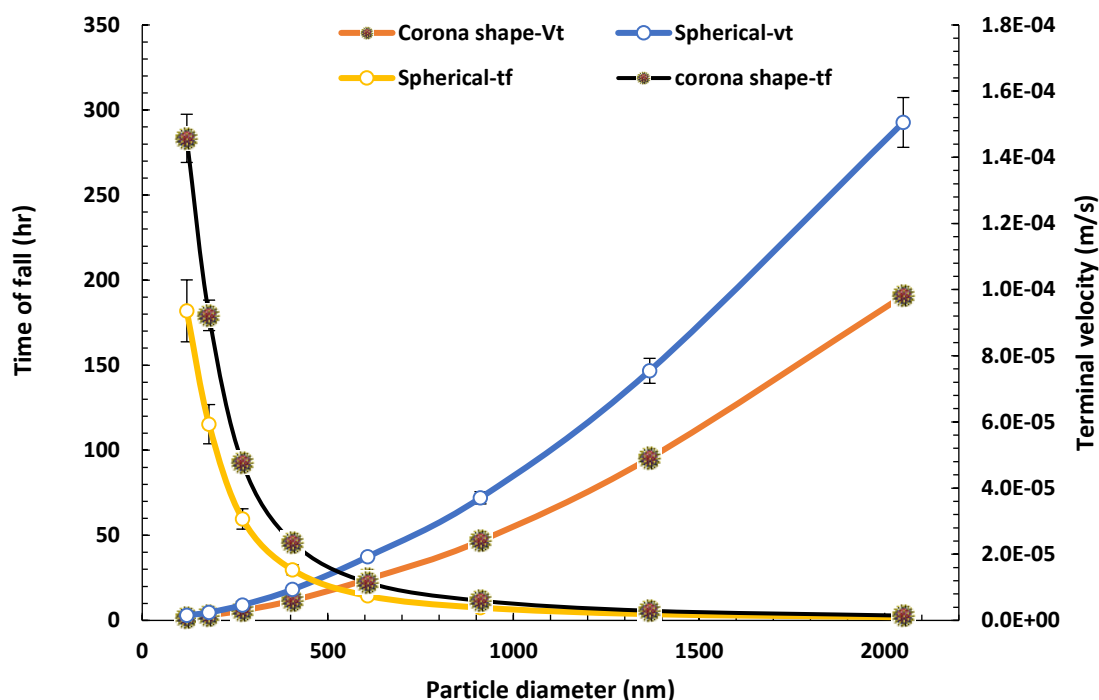
FIGURE 8 Terminal velocity and fall time of corona-shaped and spherical particles in standard atmospheric conditions.

b) Modeling the fall of corona-shaped particles in a closure

The correlations derived for drag coefficient in the previous section were applied as a UDF in FLUENT to simulate the path of particles generated by sneezing or coughing. A 3×3×5 m closure was utilized as the solution domain with a structured hexahedral computational grid of $1×10^6$ cells. Based on the findings, these nanoparticles were able to move quickly even within low-speed flows due to their high drag coefficient. They even passed the length of a 20m computational domain without any change in height, meaning falling down. Therefore, to consider the turbulence effects, the results were reported for 0.01 m/s airflow. Water-type particles with 94% volatile portion with a nanoparticle of 120 nm diameter and a density close to water, as coronavirus, were employed for the simulations. The spreading particles were sized 120 nm to 120 μm with an initial velocity of 10 m/s, which is the common flow velocity during coughing [3].

In order to investigate the effect of ambient air relative humidity on the evaporation rate of spreading particles, water mass fractions at 1 bar pressure, different relative humidities (from 0% to 100%), and various ambient temperatures were computed by a psychrometric calculator [35] and applied as the inputs and initial conditions of the model. Figure 9 compares the size change of 120 nm and 120 μm particles at two extremes of air relative humidity, namely 0% and 100%.

It is concluded that the evaporation rate decreases in higher humidity areas as there is no reduction in the particle size in saturated conditions; therefore, we can expect significantly higher terminal velocities and lower fall times [36]. The evaporation time for 1.2 μm and 120 μm particles were approximately 0.001 and 10 seconds, respectively.
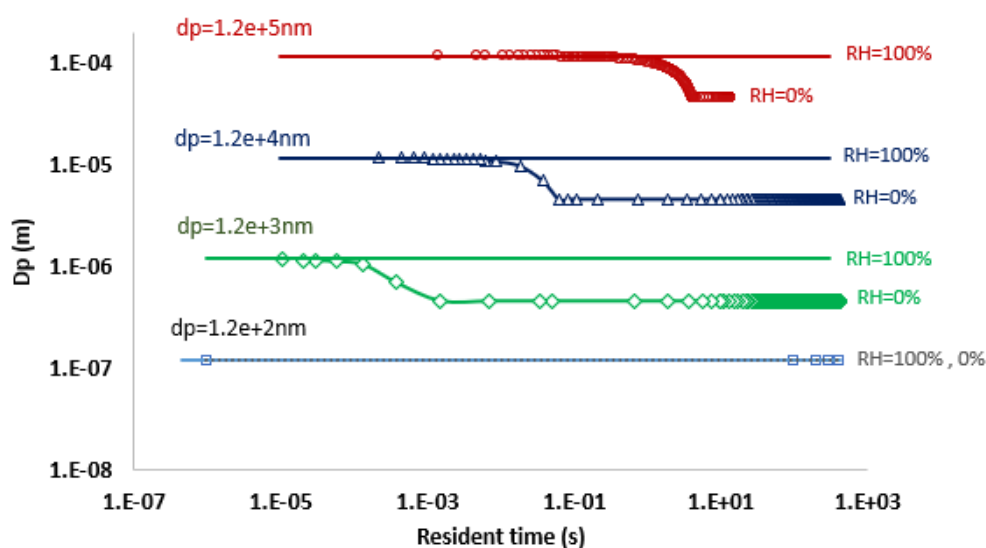
FIGURE 9 Comparison of the particles diameter changes in RH = 0% and 100%

Conclusion

In the current work, coronaviruses, with the exact dimensions of COVID-19 virus, were modeled, and their drag coefficient was determined by computational fluid dynamics (CFD). The results were compared and validated with the existing analytical correlations for spherical particles. An excellent agreement was achieved with the drag coefficient of a sphere in laminar flow(24/Re). Using derived modified correlations for the drag coefficient, terminal velocity and fall time from a 1m height were computed and compared with the spherical shape assumption. The results imply that:

1- The terminal velocity of corona-shaped particles was 10 times lower than that of the spherical ones while their fall time was longer with the same ratio due to their higher surface area to volume ratio.

2- Temperature and pressure effects were exerted by changing the dynamic viscosity and molecular free mean path. These two parameters, which influenced drag, represented different ambient conditions and elevations in the spreading location of the virus. It was concluded that terminal velocity decreased with the increase in temperature and ambient pressure (or elevation from sea level).

3- Tracking and comparing the path of virus particles in dry and wet media showed that the virus fell faster and propagated more slowly due to the lower evaporation rate of the spreading droplets carrying coronavirus in wet environments, especially saturated conditions. In contrast, in dry environments, the evaporation rate was much higher, resulting in a rapid decrease in the droplet size and an increase in the fall time, meaning a longer suspension time in the air.

Regarding the analyzed parameters and regardless of the life cycle of the virus, it could be stated that cold, high, and wet areas in particular, provided the best conditions for falling down. Accordingly, in wet areas, antisepticising the surfaces was a wise and better solution for defeating COVID-19 whereas in dry areas, antisepticising, ventilation, and filtering of air were recognized as more effective.

In this work, the life span of viruses was not considered, and all particles were assumed to be survived and not destroyed during fall. Corona particles were also assumed individually and it was assumed that no

aggregation would take place. However, it should be noted that this assumption helps to find out the worst-case results, since in the case of aggregated particles, higher weight would result into shorter fall time.

Declaration of competing interest

The authors declare that there are no conflicts of interest.

Acknowledgments

The contribution of Dr. Hossein Safari - Infectious Diseases Department, Imam Reza Hospital, Mashad University of Medical Sciences, Mashhad- is also highly appreciated by the author.

Orcid:

Mohammad Javadi: https://orcid.org/0000-0002-2818-9031

References

[1] L. Setti, F. Passarini, G. De Gennaro, P. Barbieri, M.G. Perrone, M. Borelli, J. Palmisani, A. Di Gilio, V. Torboli, F. Fontana, L. Clemente, A. Pallavicini, M. Ruscio, P. Piscitelli, A. Miani, *Environmental Research*, **2020**, *188*, 109754. [crossref], [Google Scholar], [Publisher]

[2] A.R. Sahin, A. Erdogan, P.M. Agaoglu, Y. Dineri, A.Y. Cakirci, M.E. Senel, R.A. Okyay, A.M. Tasdogan, *EJMO*, **2020**, *4*, 1-7. [crossref], [Google Scholar], [Publisher]

[3] A.A. Aliabadi, S.N. Rogak, S.I. Green, K.H. Bartlett, *In Proceedings of ASME 2010 International Mechanical Engineering Congress and Exposition*, Vancouver, Canada, **2010**, 1051-1060. [crossref], [Google Scholar], [Publisher]

[4] Y. Orooji, H. Sohrabi, N. Hemmat, F. Oroojalian, B. Baradaran, A. Mokhtarzadeh, M. Mohaghegh, H. Karimi-Maleh, *Nano-Micro Letters*, **2020**, *13*, 18. [crossref], [Google Scholar], [Publisher]

[5] W.H. Organization, **2020**. Availble at: https://www.who.int/emergencies/diseases /novel-coronavirus-2019/question-and-answers-hub/q-a-detail/coronavirus-disease-covid-19-similarities-and-differences-with-influenza

[6] L. Morawska, J. Cao, *Environ. Int.*, **2020**, *139*, 105730. [crossref], [Google Scholar], [Publisher]

[7] Contained use - Micro-organisms: Viability and susceptibility to disinfectants (Annexes). **2013**. Avalable at: https://www.biosafety.be/content/contained -use-micro-organisms-viability-and -susceptibility-disinfectants (15 may 2021).

[8] E. Cantone, R. De Luca, M. Gamerra, *Biomed. Phys. Eng. Express*, **2017**, *3*, 025017. [pdf], [Google Scholar], [Publisher]

[9] T. Nishimura, F. Mori, S. Hanida, K. Kumahata, S. Ishikawa, K. Samarat, T. Miyabe-Nishiwaki, M. Hayashi, M. Tomonaga, J. Suzuki, T. Matsuzawa, T. Matsuzawa, *PLoS Comput. Biol.*, **2016**, *12*, e1004807. [crossref], [Google Scholar], [Publisher]

[10] B.A. Craven, E.G. Paterson, G.S. Settles, *J. R. Soc. Interface*, **2010**, *7*, 933-943. [crossref], [Google Scholar], [Publisher]

[11] J. Lindemann, T. Keck, K. Wiesmiller, B. Sander, H.J. Brambs, G. Rettinger, D. Pless, *Am. J. Rhinol.*, **2006**, *20*, 219-223. [crossref], [Google Scholar], [Publisher]

[12] T. Keck, J. Lindemann, *GMS Curr. Top. Otorhinolaryngol Head Neck Surg.*, **2010**, *9*, Doc08. [crossref], [Google Scholar], [Publisher]

[13] D.Y. Wang, H.P. Lee, B.R. Gordon, *Clin. Exp. Otorhinolaryngol.*, **2012**, *5*, 181-187. [crossref], [Google Scholar], [Publisher]

[14] Y.X. Zhang, G.H. Feng, Z.Q. Kang, Y. Bi, Y.L. Cai, *Procedia Eng.*, **2017**, *205*, 302-308. [crossref], [Google Scholar], [Publisher]

[15] A. Przekwas, Z. Chen, *Med. Hypotheses*, **2020**, *144*, 110261. [crossref], [Google Scholar], [Publisher]

[16] K. Keyhani, P.W. Scherer, M.M. Mozell, *J. Biomech. Eng.*, **1995**, *117*, 429-441. [crossref], [Google Scholar], [Publisher]

[17] C.H. Lin, K.H. Dunn, R.H. Horstman, J.L. Topmiller, M.F. Ahlers, J.S. Bennett, L.M.

Sedgwick, S. Wirogo, *ASHRAE Transactions*, **2005**, 111, 755-763.

[18] E.E. Khalil, H. Kotb, *In Proceedings of AIAA Scitech Forum, Orlando*, FL, January **2020**.

[19] S. Taherian, H. Rahai, J. Bonifacio, R. Horstman, 44th AIAA Fluid Dynamics Conference June **2014**, Atlanta, GA.

[20] C.H. Chang, C.C. Chan, K.J. Cheng, J.S. Lin, *Eng. Appl. Comput. Fluid Mech.*, **2011**, *5*, 276-285. [crossref], [Google Scholar], [Publisher]

[21] Z. Fang, Z. Huang, X. Li, J. Zhang, W. Lv, L. Zhuang, X. Xu, N. Huang, *arXiv preprint arXiv*, **2020**. Available at: https://app.dimensions.ai/details/publicatio n/pub.1125168798 (17 May 2021) [Google Scholar], [Publisher]

[22] I.H. Seo, I.B. Lee, *In Proceedings of Ist International Symposium on CFD Applications in Agriculture*, **2013**, 1008, 57-62. [crossref], [Google Scholar], [Publisher]

[23] Y. Li, X. Huang, I.T. Yu, *Indoor Air*, **2005**, *15*, 83-95. [crossref], [Google Scholar], [Publisher]

[24] B. Blocken, F. Malizia, T. Van Druenen, T. Marchal, Preprint. Available at: http://www. urbanphysics. net/Social% 20Distancing% 20v20_White_Paper. pdf. Accessed April **2020**, 20.

[25] C. Lyons, M. Callaghan, *Anaesthesia*, **2020**, *75*, 843-847. [crossref], [Google Scholar], [Publisher]

[26] R. Devi, S. Gogoi, S. Barua, H.S. Dutta, M. Bordoloi, R. Khan, *Food Chem.*, **2019**, *276*, 350-357. [crossref], [Google Scholar], [Publisher]

[27] A. Haider, O. Levenspiel, *Powder Technol.*, **1989**, *58*, 63-70. [crossref], [Google Scholar], [Publisher]

[28] H. Yang, M. Fan, A. Liu, L. Dong, International Journal of Mining Science and Technology, 2015, 25, 219-223. [crossref], [Google Scholar], [Publisher]

[29] ANSYS FLUENT theory guide. Cannonsburg, PA, USA: ANSYS, Inc: **2013**.

[30] R. Miller, K. Harstad, J. Bellan, *Int. J. Multiph.*, **1998**, *24*, 1025-1055. [crossref], [Google Scholar], [Publisher]

[31] W. Ranz, W.R. Marshall, *Chem. Eng. Prog*, **1952**, *48*, 141-146. [Publisher]

[32] M.P. Wan, C.Y.H. Chao, Y.D. Ng, G.N.S. To, W.C. Yu, *Aerosol Sci. Technol.*, **2007**, *41*, 244-258. [crossref], [Google Scholar], [Publisher]

[33] M. Deevy, Y. Sinai, P. Everitt, L. Voigt, N. Gobeau, *Energy Build.*, **2008**, *40*, 255-264. [crossref], [Google Scholar], [Publisher]

[34] H. Qian, Y.G. Li, P.V. Nielsen, X.H. Huang, *Build. Environ.*, **2009**, *44*, 1651-1658. [crossref], [Google Scholar], [Publisher]

[35] Megawatsoft: HumidAir Desktop Application. available at: https://www.megawatsoft.com/

[36] L. Morawska, J.W. Tang, W. Bahnfleth, P.M. Bluyssen, A. Boerstra, G. Buonanno, J. Cao, S. Dancer, A. Floto, F. Franchimon, C. Haworth, J. Hogeling, C. Isaxon, J.L. Jimenez, J. Kurnitski, Y. Li, M. Loomans, G. Marks, M. Yao, *Environ. Int.*, **2020**, *142*, 105832. [crossref], [Google Scholar], [Publisher]